Soft Matter

Accepted Manuscript

ROYAL SOCIETY OF CHEMISTRY

www.rsc.org/softmatter

Soft Matter

ARTICLE

Gelation of Fmoc-diphenylalanine is a first order phase transition†

Nikola A. Dudukovic[*a] and Charles F. Zukoski[b]

Received 00th January 2015,
Accepted 00th January 2015

DOI: 10.1039/x0xx00000x

www.rsc.org/

We explore the gel transition of the aromatic dipeptide derivative molecule fluorenylmethoxycarbonyl-diphenylalanine (Fmoc-FF). The addition of water to a solution of Fmoc-FF in dimethyl sulfoxide (DMSO) results in increased attractions leading to self-assembly of Fmoc-FF molecules into a space-filling fibrous network. We provide evidence that gel formation is associated with a first order phase transition resulting in nucleation and growth of strongly anisotropic crystals with high aspect ratios. The strength of attraction between Fmoc-FF molecules as a function of water concentration is estimated from long-time self-diffusion measurements using ^{1}H NMR diffusion-ordered spectroscopy (DOSY). The resulting phase behavior follows that observed for a wide range of other crystallizing nanoparticles and small molecules – a result consistent with the short-range nature of the intermolecular attractions. Furthermore, we use NMR to measure the rate of increase in the fraction of bound Fmoc-FF molecules after water is suddenly mixed into the system. We observe a lag time in the formation of the new phase indicative of the existence of a free energy barrier to the formation of a crystal nucleus of critical size. The application of classical nucleation theory for a cylindrical nucleus indicates that one-dimensional crystal growth is driven by an imbalance of the surface energies of the ends and sides of the fiber.

Introduction

Molecular gels are formed from the self-assembly of molecules experiencing hydrogen bonding and π-π stacking interactions into anisotropic structures, typically fibers of high aspect ratios, which produce space-spanning networks that resist shear, resulting in a bulk material with properties characteristic of soft solids.[1,2] A specific class of molecular gels that has gained considerable attention over the past decade are self-assembling systems based on short peptide derivatives, which form ordered fibrous structures, usually based on π-π stacking of ß-sheets.[3] The most widely studied such molecule is the dipeptide fluorenylmethoxycarbonyl-diphenylalanine (Fmoc-FF).[4-12] Addition of water to low-concentration solutions of this molecule in dimethyl sulfoxide (DMSO) results in the formation of mechanically and thermally reversible gels with long relaxation times and substantial elastic moduli.[9-12] Due to ease of chemical modifications, Fmoc-FF and similar gelators provide opportunities to design materials with unique structural, optical, mechanical and biological functionalities.[3] The gelation mechanism in these types of systems remains poorly understood, limiting the general design of new molecules and the engineering of new products based on these molecular gels for applications in tissue engineering, drug delivery, nanofabrication, biosensing, etc.[13-16]

Here we provide evidence that, when exposed to water, Fmoc-FF molecules in DMSO undergo a first order phase transition to form crystalline fibers of high aspect ratios. This crystalline morphology arises from anisotropic molecular interactions that give rise to substantial differences in surface tension at the ends and sides of the resulting crystals. Due to limitations of rates of mixing, upon initial addition of water very high strengths of attraction are achieved, resulting in the formation of a metastable phase that is subsequently displaced by fiber formation.[17] This initial phase is amorphous, and the ensuing formation of an ordered phase indicates that the crystalline phase has the lower free energy. Our results suggest that the soft solid mechanical response of the gels arises from the low number density of intermolecular (physical) bonds, and the ease of repairing structures damaged by mechanical disruption through rapid dissolution and recrystallization processes is enabled by high surface areas of the crystals.

To build the case that Fmoc-FF molecules undergo a first order phase transition in forming fibers, we first seek to move from a description of gel line denoted by concentrations of water and Fmoc-FF at the gel point (**Figure 1**) to a phase diagram where water concentration is converted to an effective strength of intermolecular interaction and a phase diagram where transitions can be denoted in terms of the strength of attraction between Fmoc-FF molecules and the Fmoc-FF concentration. With this information in hand, we demonstrate that the phase boundary of this molecule can be mapped onto generalized phase behavior seen for a variety of molecules and colloidal particles that experience isotropic and

[a] Department of Chemical and Biomolecular Engineering, University of Illinois at Urbana-Champaign, Urbana, IL 61801, USA. Email: dudukov1@illinois.edu.
[b] Department of Chemical and Biological Engineering, University at Buffalo, Buffalo, NY 14222, USA.

† Electronic Supplementary Information (ESI) available: full NMR spectra, detailed calculations, and additional kinetics data. See DOI: 10.1039/x0xx00000x

weakly anisotropic attractions. We further demonstrate that at constant strength of attraction, two phases are in equilibrium as the average concentration of the Fmoc-FF molecule is increased above the phase transition concentration. Finally, we show that there is a weak barrier to crystal nucleation and discuss this barrier in terms of the quasi-one-dimensional crystal nucleation that takes place in the studied system.

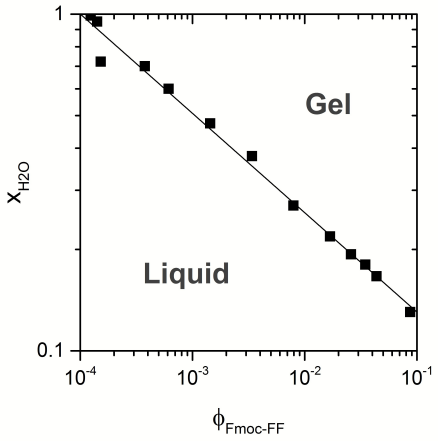

Figure 1. Gel line of Fmoc-FF/DMSO/H_2O system. Volume fractions of Fmoc-FF are determined as given in Eqs. (2) and (3).

Below, we first describe theoretical and experimental studies of the phase behavior of small molecules and nanoparticles and how diffusivities can be used to characterize strength of interparticle attractions. We then proceed to describe our experimental methods and discuss our results where we link diffusion to strength of attraction and strength of NMR signal to freely diffusing molecule concentration. Finally, we draw conclusions about the phase behavior of the gelator in the Fmoc-FF/DMSO/H_2O system and propose the appropriate phase diagram.

Phase behavior of nanoparticles and small molecules

Detailed theoretical, simulation and experimental studies suggest that short-range isotropic attractions result in a phase diagram where liquid-liquid phase separation is always metastable relative to a fluid-crystal phase boundary.[18-20] The spinodal defining a dilute-concentrated or liquid-liquid phase separation (analogous to a gas-liquid phase transition for single component systems) is metastable and occurs at concentrations larger (temperatures lower) than the crystallization boundary. Studied extensively for colloidal particles and proteins (diameters greater than 50 nm), the generalized nature of these phase transition boundaries has been extended to small molecules and proteins experiencing anisotropic interactions.[21-27] The presence of the metastable liquid/liquid phase separation has been seen in proteins and small molecule systems. These studies suggest that at the same average strength of attraction, broad classes of Brownian particles display very similar solubilities.[27-30] The metastable spinodal appears more sensitive to details of the molecular interactions than is the solubility.[25,31]

Gelation in colloidal and protein solutions has been associated with rapid quenches into the spinodal of metastable liquid-liquid phase boundary that exists for particles experiencing short-range attractions. The increased mechanical strength of the gels is associated with low particle diffusivity in the dense, amorphous state resulting in aggregation of clusters into space-spanning structures. Aging and ultimate crystallization of these gels is then expected (and observed) as the system slowly relaxes into the lowest free energy minimum of a crystal in equilibrium with a dilute molecular solution. The key features we draw from this experimental and theoretical work are:

(1) When molecules experience short-range attractions, as the strength of attraction is increased or the temperature is lowered, molecules will spontaneously phase separate into crystalline and dilute amorphous phases.

(2) At the same average strength of attraction, broad classes of molecules have the same solubility and a coexistence region exists that follows a lever arm rule relating the average concentration of the solute to the volume of the two equilibrium phases.

(3) The formation of the crystal phase is associated with a nucleation event where there is a free energy barrier that must be transversed to form a critical nucleus. The existence of this barrier can be inferred by the existence of a delay time associated with crystal formation after a rapid quench to higher attractions or lower temperatures.

(4) If the quench is strong enough, a metastable phase separation can take place which, given enough time, will relax into the equilibrium phases.

We explore the application of these ideas to the Fmoc-FF/DMSO/H_2O system. As the water concentration is decreased, higher Fmoc-FF concentrations are required to see a gel (**Figure 1**). Furthermore, at fixed Fmoc-FF volume fraction, increasing the amount of water in the system results in increased elasticity. These observations clearly indicate that water is responsible for increased attractions between the Fmoc-FF molecules and that there is a change of state of the Fmoc-FF molecules over a narrow change in water concentration. Previously, we demonstrated that the Fmoc-FF gel is reversible with respect to yielding upon intense mechanical agitation and melting with increases in temperature.[17,32] The fibers are observed to form and fluctuate in local concentration over relatively short periods of time (minutes to hours).[33]

Fmoc-FF is hydrophobic and insoluble in water, but dissolves to very high concentrations in DMSO (volume fractions approaching 0.5), resulting in stable solutions. In the presence of water, the peptide backbones form hydrogen bonds necessary to create beta sheets, while the aromatic nature of fluorenyl group and the amino acid side groups allow for π-π stacking interactions,[5] which are highly anisotropic and short-range relative to the size of the Fmoc-FF molecule. Compact or chunky crystals are not formed when water is added to an Fmoc-FF/DMSO solution. Nevertheless, the produced fibers are ordered,[5] suggesting that they can be treated as an equilibrium crystalline state formed from

anisotropic particles experiencing short-range interactions. We explore this hypothesis by comparing the phase behavior of the Fmoc-FF/DMSO/H_2O system to other systems experiencing generalized phase behavior.

This is done in several ways. First, we make a connection to previous studies showing that a wide variety of organic and inorganic molecules show very similar phase behavior when their solubilities are compared at the same average strength of attraction. Second, we show that the lever arm rule is operational in the gelled state. Finally, we measure the induction time for the formation of the fiber phase and again show consistency with classical nucleation theories used to describe phase transitions of small molecules and colloids. Each of these studies provides evidence that the Fmoc-FF/DMSO/H_2O system undergoes a first order phase transition to form a highly anisotropic crystalline phase and that the large clusters observed in solution on rapid mixing with water are indicative of a quench into the spinodal of a liquid-liquid phase separation that relaxes with time towards an ultimate equilibrium state.

Characterizing strength of attraction using self-diffusivity

The volume fraction dependence of the long-time self-diffusivity of Fmoc-FF carries information about molecular interactions. The molecules diffuse more slowly if they spend time in close proximity where they are more strongly hydrodynamically coupled. Intermolecular attractions increase the time molecules spend at small separations, thus further slowing the rate of diffusion. In the dilute limit, assuming the molecules are spheres, the long-time self-diffusion coefficient, D_S, is a linear function of molecule volume fraction:[34-36]

$$D_S \cong D_0(1+D_2\phi) \qquad (1)$$

where $D_0 = kT/6\pi\mu a$ is the Stokes-Einstein diffusivity assuming no-slip solid/fluid boundary conditions, ϕ is the molecule volume fraction, while D_2 reflects hydrodynamic interactions between pairs of particles. If the particles experience attractions, the pair distribution will be altered such that pairs spend more time at smaller separations. Stronger hydrodynamic coupling at small separations results in smaller values of D_2 (i.e. D_2 becomes more negative). As discussed later on, we assume that under the dilute conditions, the particle pair distribution function is well approximated as $g(r) = \exp[-u(r)/kT]$ for $r > \sigma$, where $u(r)$ is the pair interaction energy for particles of diameter σ with center-to-center separation r. For $u(r)$ we use a square well potential and assume the particles are spheres and interact with hydrodynamic mobility functions $A_{ij}(r)$ and $B_{ij}(r)$ for particles experiencing no-slip boundary conditions[34,35] (see supplementary information, ESI†). With these approximations we are able to use measurement of volume fraction dependent diffusivities to extract an estimate of interparticle attraction. As the particles experience anisotropic interactions, but are Brownian, we expect the average strength of attraction extracted from our approximations to be weighted towards the largest strength of attraction.

Experimentally, D_S can be measured using pulsed field gradient spin echo nuclear magnetic resonance (PFGSE NMR), employing diffusion-ordered spectroscopy (DOSY) measurements based on PFGSE sequences. The advantages of NMR spectroscopy are that it can be used to measure diffusion of small molecules, as well as its ability to provide signals o different molecules in the solution even at low concentrations.

While we determine D_2 in the dilute limit where D_s is a linear function of ϕ, we investigate translational diffusion in Fmoc-FF solutions at conditions approaching and above the gelation boundary and measure the gelation kinetics of slowly gelling samples using ^{1}H NMR spectroscopy. We use the changes in static ^{1}H NMR signal intensity over time as a measure of the conversion of Fmoc-FF molecules into solid structures in the gel. Using the obtained data, we explore the hypothesis of Fmoc-FF fibers being an equilibrium crystalline state and develop a phase diagram for the Fmoc-FF/DMSO/H_2O system using simple fluid diffusion models and crystallization theories.

Experimental methods

Materials and sample preparation

Solid Fmoc-FF powder was purchased from Bachem (Bubendorf, Switzerland) and used without further purification. Dimethyl sulfoxide (99.5%, Sigma-Aldrich) and Milli-Q water were used in sample preparation for rheology measurements. For NMR measurements, deuterated solvents were used (deuterium oxide, D_2O, and deuterated DMSO, $(CD_3)_2S=O$), obtained from Cambridge Isotope Laboratories Inc. For clarity and consistency purposes, the deuterated solvents will be referred to simply as DMSO and H_2O throughout the text. Fmoc-FF was dissolved in DMSO at the desired volume fractions, calculated by:

$$\phi_{Fmoc-FF} = \frac{V_{Fmoc-FF}}{V_{Fmoc-FF}+V_{DMSO}+V_{H_2O}} \qquad (2)$$

$V_{Fmoc\text{-}FF}$ is related to the measured mass of Fmoc-FF ($m_{Fmoc\text{-}FF}$):

$$V_{Fmoc-FF} = \frac{N_A m_{Fmoc-FF}}{M_{Fmoc-FF}} V_{molecule} \qquad (3)$$

where N_A is Avogadro's number, $M_{Fmoc\text{-}FF}$ = 534.61 g/mol is the molar mass and $V_{molecule}$ = 0.487 nm^3 is the estimated volume of a single Fmoc-FF molecule.[36]

^{1}H NMR gelation kinetics measurements

All NMR measurements were performed on a 750 MHz Agilent VNMRS NMR spectrometer, equipped with a 5 mm Varian ^{1}H{^{13}C/^{15}N} PFG XYZ probe. The instrument was operated in liquid-state mode and controlled using VNMRJ software v3.2A. Compositions near the gel point were chosen at water concentrations x_{H2O} = 0.25-0.40 (**Figure 1**), ensuring a

sufficiently long gelation time to allow mixing and transfer to the NMR tubes (≥ 0.5 hours).

The solution was mixed with deuterium oxide and 700 µL was transferred into a 5 mm thin wall precision NMR sample tube (Wilmad-LabGlass). The sample tube was immediately placed into the NMR instrument and the collection of ^{1}H spectra at selected time intervals was commenced. The first ^{1}H spectrum was taken as the reference of the fully liquid state at time t = 0 for each sample. The final conversion to solid of each sample was determined from the ^{1}H spectrum taken after 14 days from the starting measurement. All spectra were taken at a pulse width of 90º.

^{1}H DOSY (PFGSE) NMR measurements

The self-diffusion coefficients were measured using the DOSY capabilities of the 750 MHz Agilent VNMRS instrument. The experiments were performed with liquid solutions at various Fmoc-FF volume fractions in both pure deuterated DMSO and solutions with deuterated water concentrations $x_{H2O} \leq 0.40$. PFGSE NMR utilizes the attenuation of the echo signal from a spin-echo pulse sequence containing a magnetic field gradient pulse at each period to determine the displacement of the observed spins on timescales of milliseconds to seconds.[38,39] The self-diffusivity of the spins can then be correlated to the attenuation of the spin echo signal (see ESI† for technique details).

Rheology Measurements

Rheology experiments were performed on a TA Instruments DHR-3 rheometer with a Peltier plate and solvent trap, using a 4º/40 mm cone geometry. Fmoc-FF/DMSO solutions were prepared as previously described. As soon as water was added to the solution in a vial, the sample was mixed lightly and 1.2 mL of the mixture was quickly transferred onto the rheometer. The rotating element was lowered into the measurement position and the experiment was started immediately. The evolution of the elastic modulus with time was measured at 25 ºC, at an oscillating strain of 0.005 and frequency 1 Hz.

Results and Discussion

The diffusion coefficients of Fmoc-FF in solution were determined from the exponential decays of the peak intensities (**Figure 2**). The measured diffusivities decrease with increasing Fmoc-FF volume fraction (**Figure 3a**) and increasing water concentration (**Figure 3b**). The data shown in **Figure 3** represent the diffusive behavior of Fmoc-FF molecules in fully liquid solutions at compositions below the gel point. The values of D_0 vary systematically with water concentration as expected for an increase in viscosity of the DMSO/H_2O mixture[40] and the Stokes-Einstein expression for no-slip boundary conditions ($D_0 = kT/6\pi\mu a$) holds, suggesting a constant hydrodynamic radius of 0.63±0.05 nm (**Figure 3b**). This is in relatively good agreement with the radius estimated for a hard sphere from simulated molecular volume ($V_{molecule}$ = 0.487 nm^3, $a_{molecule}$ = 0.49 nm). The disagreement a result of the assumption that the Fmoc-FF molecule is a sphere (a better approximation would be a spheroid) and the fact that some solvent adsorption is expected on surface the molecule, thereby increasing its hydrodynamic size.[41] As expected, the diffusivity decreases with increasing Fmoc-FF concentration, and at higher rates as water concentration increases. When normalized by D_0 following Eq. (1), the line slopes of D_S/D_0 vs. $\phi_{Fmoc\text{-}FF}$ in **Figure 4** correspond to D_2.

As discussed in the introduction, D_2 can be used as a surrogate for the strength of pair interactions with more negative values indicating stronger pair attractions. Our results in **Figure 4** thus suggest increasing strength of attraction with increasing water concentration. Greater strengths of attraction are associated with lower solubilities and previous studies have demonstrated that a range of molecules show similar solubilities at the same value of D_2.[27]

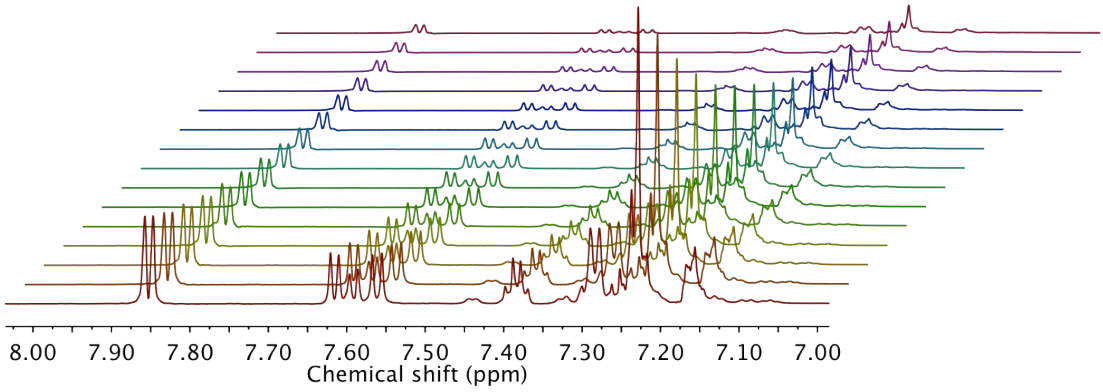

Figure 2. ^{1}H DOSY spectra of Fmoc-FF in pure DMSO ($\phi_{Fmoc\text{-}FF}$ = 0.027). The peaks shown correspond to the aromatic protons of the molecule (see Figure S1, ESI† for full spectrum).

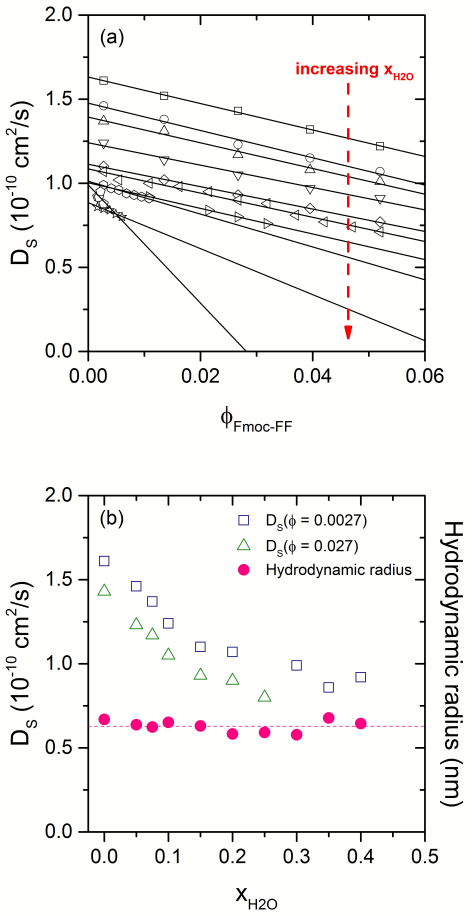

Figure 3. (a) Self-diffusivity D_S obtained from ^{1}H DOSY NMR as a function of Fmoc-FF volume fraction for various water concentrations; **(b)** Self-diffusivity as a function of water concentration at two Fmoc-FF volume fractions (one order of magnitude apart).

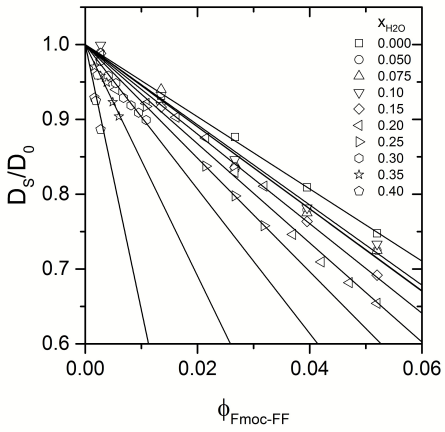

Figure 4. Diffusion coefficients D_S measured by ^{1}H DOSY NMR scaled by D_0 for different water concentrations. The slopes of the lines correspond to the pair contribution of the scaled self-diffusivity D_2, as according to Eq. (1).

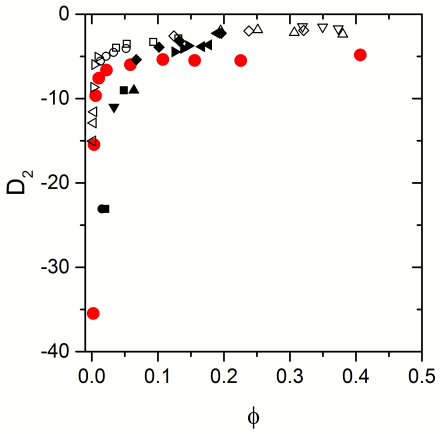

Figure 5. Red circles: self-diffusivity D_2 of Fmoc-FF as a function of solubility ϕ for wa concentrations $x_{H2O} \leq 0.40$; other symbols: generalized phase diagram data taken from He *et al.*[27]

Figure 5 shows a plot of D_2 as a function of Fmoc-FF volume fraction at the gel point for water concentrations $x_{H2O} \leq 0.40$. As shown, the data obtained for Fmoc-FF compares well with that of He *et al.*[27] for the crystallization boundary of a variety of small molecules in different solvents. These results demonstrate that Fmoc-FF follows the phase behavior of other crystallizing nanoparticles and molecules such as amino acids and globular proteins. We note difficulties in making direct comparisons with the data of He *et al.* due to employment of different methods of determining molecular volume. Changes in molecular volume impact the absolute value of D_2 and volume fraction. The comparison given in **Figure 5** shows remarkable agreement in phase behavior for a very wide set of organic and inorganic molecules providing some confidence that even with its highly anisotropic pair interactions, Fmoc-FF can be treated as particle experiencing short range attractions with the physical chemistry very similar to that seen in less anisotropic systems. Further comparisons require linking D_2 to an average strength of attraction. This is done by assuming continuum approximations for the long time self-diffusivity. Let us assume that Fmoc-FF molecules can be treated as spherical particles.

The repulsive and attractive forces can be described by a square well potential of strength of interaction ε and range o interaction δ:

$$u(r) = \begin{cases} \infty & r < \sigma \\ -\varepsilon & \sigma \leq r < \sigma(1+\delta) \\ 0 & r \geq \sigma(1+\delta) \end{cases} \quad (4)$$

If the center-to-center separation is normalized by the parti radius such that $r^* = 2r/\sigma$ and δ is taken as the measure of the range, then D_2 can be written as:[27,35]

$$D_2 = \int_2^\infty (-3 + A_{11} + 2B_{11}) g(r^*) r^{*2} + \int_2^\infty \left[\frac{A_{11} - A_{12} - B_{11} + B_{12}}{r^*} + \frac{1}{2}\left(\frac{dA_{11}}{dr^*} - \frac{dA_{12}}{dr^*} \right) \right] Q(r^*) g(r^*) r^{*2} dr^* \quad (5)$$

where in the dilute limit $g(r^*) = \exp[-u(r^*)/kT]$, A_{ij} and B_{ij} are hydrodynamic mobility functions of r^*, and $Q(r^*)$ is the perturbation of the pair distribution function.[34] The first term in Eq. (5) represents the short-time self-diffusivity correction, while the second term is the correction for long-time diffusion. The numerical solutions of A_{ij}, B_{ij} and $Q(r^*)$ are given by Batchelor[34] and Jeffrey and Onishi[35] (see ESI† for equations).

By taking the characteristic spacing between the peptide backbones (0.48 nm)[5,17] as the measure of the range of interaction, we can estimate the strength of attraction by setting $\delta = 0.2$. Thus we find the relationship between water concentration and the strength of attraction (**Figure 6a**) and plot kT/ε as a function of the solubility (**Figure 6b**, red circles). The faster-than-exponential dependence of ε/kT in **Figure 6a** shows that the strength of attraction is highly sensitive to water concentration. We attribute the appearance of the large amorphous clusters seen in initial mixing of water with Fmoc-FF/DMSO solutions to local water concentrations exceeding 0.4 where kT/ε drops dramatically. These conditions can be expected to push the solution into the spinodal where Fmoc-FF molecules will diffuse up concentration gradients and rapidly form clusters.

Further evidence for the crystallization of the Fmoc-FF molecule can be drawn from determining that there is a coexistence region below and to the right of the solubility boundary in **Figure 5**. At fixed D_2 (fixed strength of attraction), as the average volume fraction of Fmoc-FF in the system is increased, at equilibrium we expect that concentration of freely diffusing Fmoc-FF to remain a constant while the volume of the solid phase increases. We determine the concentration of freely diffusing Fmoc-FF using NMR measurements performed in liquid-state mode as the resulting signal is not responsive to non-diffusive molecules. Therefore, the concentration of free molecules in solution can be determined inside a metastable coexistence region, which can be defined by the peak area ratios.

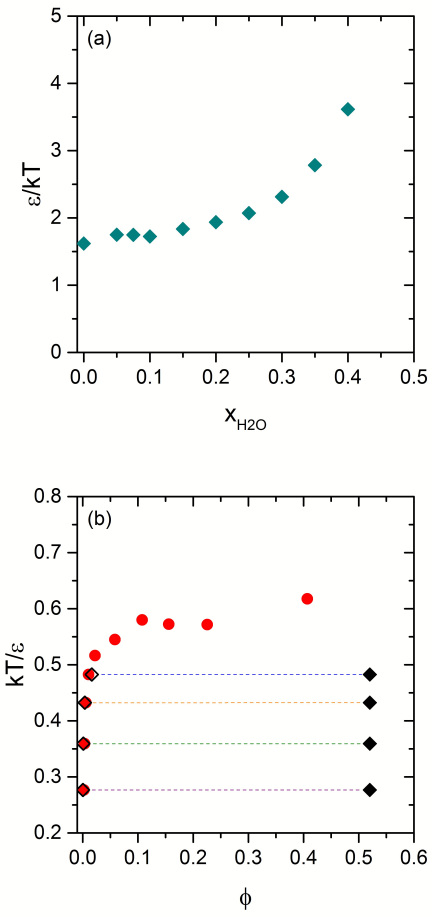

Figure 6. (a) Dependence of the strength of attraction ε/kT on water concentration; **(b)** Phase diagram: red circles – liquid phase boundary evaluated from D_2 measurements; hollow and full diamonds – liquid and solid boundaries determined using the lever rule in Eq. (8).

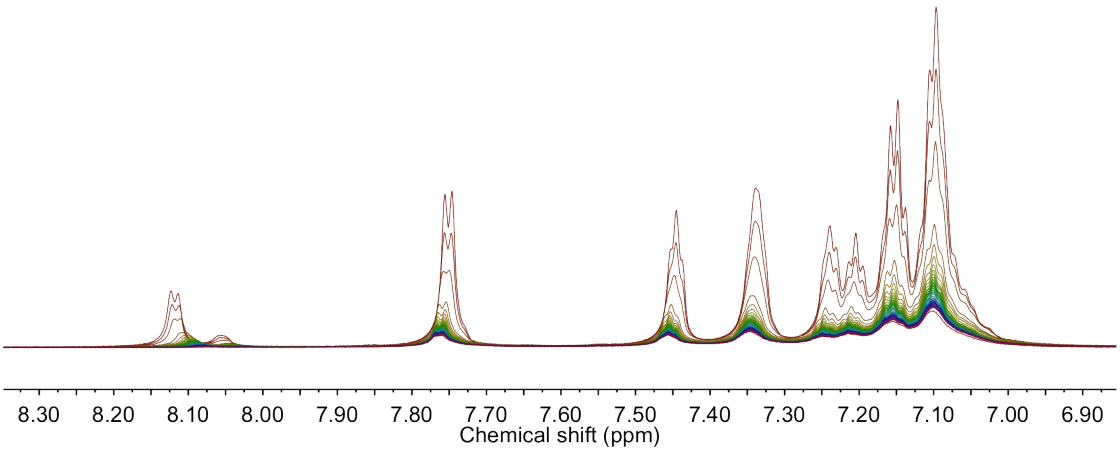

Figure 7. Decrease in NMR signal intensity with time during gelation of Fmoc-FF ($\phi_{Fmoc\text{-}FF} = 0.027$; $x_{H2O} = 0.35$); the areas under the peaks are proportional to the total number of spins in the liquid.

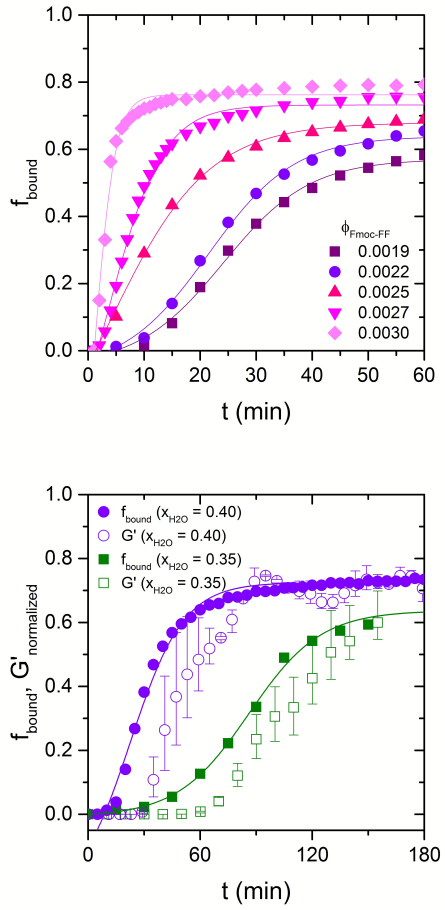

Figure 8. (a) Fraction of Fmoc-FF molecules bound in the solid phase (x_{H2O} = 0.35) as a function of time calculated using Eq. (6); the solid lines are fits to a Boltzmann-type sigmoidal function given in Eq. (9). **(b)** Comparison between gelation kinetics measured by NMR and rheology for $\phi_{Fmoc\text{-}FF}$ = 0.002 at two water concentrations.

The fraction of molecules bound in solid structures at time t was calculated from the peak area A, using the spectrum taken at time t_0 as a reference for the fully liquid state and averaging over n Fmoc-FF peaks:

$$f_{bound} = \sum_{i=0}^{n}\left(1-\frac{A_i(t)}{A_i(t_0)}\right) \qquad (6)$$

Figure 7 shows spectra as a function of time for the frequency shift region associated with the aromatic features of Fmoc-FF. Over time, the peak intensities and areas under the peaks decrease. Averaging over all Fmoc-FF peaks, we estimate the fraction of Fmoc-FF that is in a solid-state structure. The data is summarized in **Figure 8a**, which indicates that there is an induction time associated with the low probability processes leading to the formation of fibers, i.e. a nucleation event. These kinetic curves qualitatively follow the rheology kinetics measured at the same conditions (**Figure 8b**). The lagging of the modulus evolution curves compared to the crystal growth curves is due to the fact that the onset of macroscopic solid-like behavior arises from interconnecting fibrous clusters, whereas the induction time in the f_{bound} curves corresponds to the formation of a critical nucleus.

At long times, as shown in **Figure 8a**, the bound fraction of Fmoc-FF molecules reaches a constant value. We evaluated the conversion to solid as the f_{bound} of each sample determined at 14 days from the starting measurement. It is evident from **Table 1** that, even at long times, not all of the peptide molecules are bound. We note that the self-diffusivity of the freely diffusing Fmoc-FF molecules does not change significantly from the values seen before the gel transition takes place, indicating that they diffuse as monomers in the gelled state (Figure S4, ESI†). This fraction of unbound molecules suggests that the system reaches an equilibrium, as expected for a material in a solid-liquid coexistence region. If this is the case, a lever rule can be applied to determine the liquid and solid phase boundaries (ϕ_L and ϕ_S) in the phase diagram:

$$\frac{V_S}{V_T} = \frac{\phi-\phi_L}{\phi_S-\phi_L} \qquad (7)$$

where V_S and V_T are the volume of the solid phase and total volume, respectively. We assume the volume fraction in the solid phase is that of densely packed Fmoc-FF molecules at a volume fraction of ϕ_{max}. Here we choose $\phi_S = \phi_{max} = 0.52$ (that for packing of hard spheres in a Bernal spiral),[42,43] although the exact choice makes little difference to determination of ϕ. Eq. (7) can be re-written such that the product of Fmoc-FF volume fraction and fraction of bound molecules is a linear function of ϕ, in which the slope and intercept are functions of ϕ_L and ϕ_S (**Figure 9**):

$$\phi f_{bound} = \frac{\phi_S}{\phi_S-\phi_L}\phi - \frac{\phi_S\phi_L}{\phi_S-\phi_L} \qquad (8)$$

Of particular interest in **Figure 9** is that plots of ϕf_{bound} versus ϕ are well approximated by straight lines. The slopes of these lines are close to unity, indicating $\phi_L/\phi_S << 1$. The linearity of the data indicates that in the two-phase region, as the average concentration of Fmoc-FF is increased, ϕ_S and ϕ_L are constant and only the volumes of the solid and liquid phases change. We extract ϕ_L and compare this measure of the solubility with that determined from the gel points, and we see superposition (**Figure 6b**). These results are strongly suggestive of the coexistence of equilibrium phases in the gelled state.

Table 1. Fraction of bound Fmoc-FF molecules after 14 days.

x_{H2O} = 0.25		x_{H2O} = 0.30		x_{H2O} = 0.35		x_{H2O} = 0.40	
ϕ	f_{bound}	ϕ	f_{bound}	ϕ	f_{bound}	ϕ	f_{bound}
0.027	0.37	0.011	0.68	0.003	0.58	0.0016	0.7(
0.032	0.57	0.014	0.77	0.004	0.78	0.0019	0.83
0.037	0.68	0.016	0.81	0.005	0.83	0.0022	0.83
0.042	0.74	0.019	0.84	0.007	0.88	0.0025	0.86
0.047	0.69			0.009	0.88	0.0027	0.8(

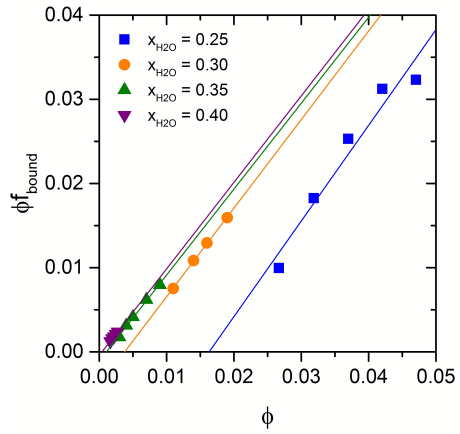

Figure 9. The product of fraction of bound molecules and total Fmoc-FF volume fraction as a function of $\phi_{Fmoc\text{-}FF}$ calculated from ^{1}H NMR data.

When water is mixed with the Fmoc-FF/DMSO solution, there is a delay before fibers are observed and a fraction of Fmoc-FF no longer freely diffuses. The resulting lag times shown in **Figure 8a** are indicative of a nucleation process where there is a free energy barrier to the formation of the solid phase. The measured induction times range from minutes to hours (more data available in Figure S3, ESI†) and decrease with increasing Fmoc-FF and water concentrations. We extract induction times from the data by first fitting the curves in **Figure 8a** to a Boltzmann-type sigmoidal function of the form:

$$f_{bound} = f_{sat} + \frac{f_0 - f_{sat}}{1+\exp((t-t_c)/dt)} \quad (9)$$

where f_0 and f_{sat} are the lower and upper plateau (fractions of bound molecules at time t_0 and at time t where f_{bound} saturates), respectively, t_c denotes the position of the center of the linear slope, and dt is a time constant. We then find the induction time t_{ind} at the point where the linear slope (where $f_{bound} = (f_0 - f_{sat})/4dt$) and the lower plateau would meet:

$$t_{ind} = \frac{4dt\, f_0}{f_{sat} - f_0} - 2dt + t_c \quad (10)$$

We note that as the supersaturation $S = \phi/\phi_L$ increases, induction time t_{ind} decreases. This behavior is reminiscent of crystal nucleation, where concentration fluctuations are needed to exceed a free energy barrier for the crystal phase to grow.

Following classical nucleation theory, the free energy of formation of a solid phase of surface A is given by a sum of a negative bulk term and positive surface term:[25,44-46]

$$\Delta G = n\Delta\mu + A\alpha \quad (11)$$

where n is the number of monomers, $\Delta\mu = -kT\ln S$ is the change in chemical potential on forming the nucleus, $S = \phi/\phi_L > 1$ is the supersaturation, and α is the crystal-liquid surface tension. For a spherical nucleus, the bulk term decreases with nucleus size as R^3 and the surface term increases as R^2:

$$\Delta G = -\frac{4/3\pi R^3}{4/3\pi a^3} kT\ln S + 4\pi R^2\alpha \quad (12)$$

The terms in Eq. (7) can be made dimensionless by the particle radius a and kT so that:

$$\Delta G^* = -R^{*3}\ln S + 4\pi R^{*2}\alpha^2 \quad (13)$$

The free energy barrier to nucleation is defined by $d(\Delta G^*)/dR^* = 0$ at a dimensionless critical radius R_c^*:

$$R_c^* = \frac{8\pi\alpha^*}{3\ln S} \quad (14)$$

Assuming that the induction time is a measure of the probability of a fluctuation resulting in the formation of a critical nucleus, the appropriate expression can be written as:

$$t_{ind} = B\exp(\Delta G_c^*) \quad (15)$$

where B is a pre-exponential factor characterizing the rate of nucleation and ΔG_c^* is the height of the free energy barrier evaluated at the critical size of the nucleus R_c^*. Experimentally, we determine induction times from the kinetics measured by ^{1}H NMR for a range of supersaturations (**Figure 10a**). The surface tension α^* can be found from the slope of the linearized function derived from Eqs. (13) and (15):

$$\ln t_{ind} = \frac{1}{2}\left(\frac{8\pi}{3}\right)^3 \alpha^{*3}\frac{1}{(\ln S)^2} + \ln B \quad (16)$$

This function is plotted for four different water concentrations in **Figure 10b**. The corresponding critical nucleus size is then calculated from Eq. (14). For short-range interactions, the strength of attraction can be related to the surface tension by:[25]

$$\alpha^* = \frac{\sqrt{3}}{(1+b\delta)^2}\frac{\varepsilon}{kT} \quad (17)$$

where b is a constant < 1. **Figure 10c** shows the surface tensions determined from induction times for a spherical nucleus approximation given by Eq. (16), as a function of ε/kT obtained from D_2 measurements (**Figure 6a**), with comparisons to literature data for a number of crystallizing systems.[25] We note that the surface tensions we obtain by using Eq. (16) are substantially lower than those observed in other systems, suggesting the barrier to nucleation is unexpectedly small. In making these comparisons, we emphasize that we are comparing systems that have the same solubilities at the same average strength of attractions, as indicated in **Figure 5**. As a result, we seek an explanation in the details of this Fmoc-FF system that differentiates it from the other systems with such similar equilibrium behavior.

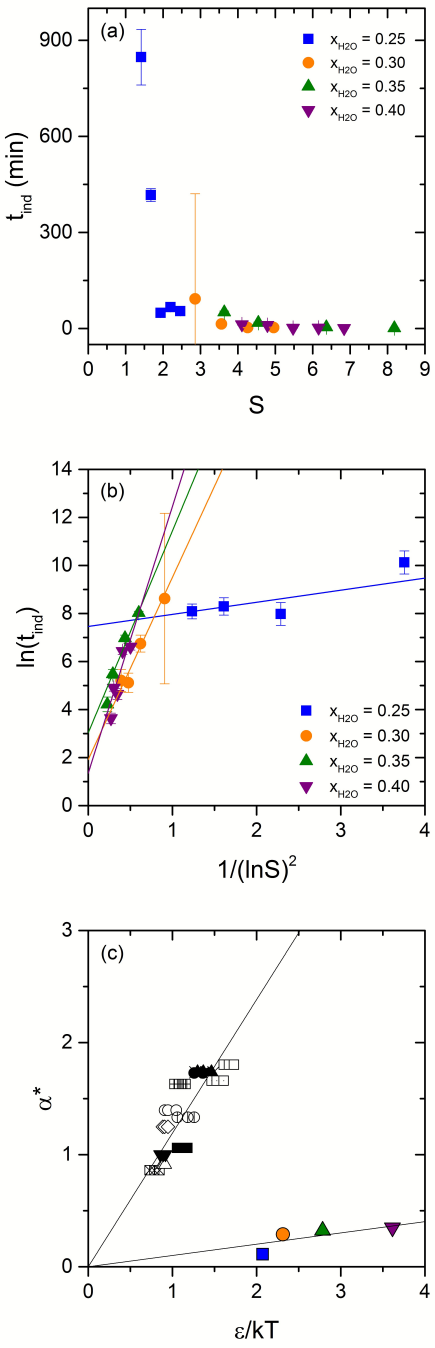

Figure 10. (a) Induction times determined from fits of $f_{bound}(t)$; **(b)** Linearized functions of t_{ind}; **(c)** Dimensionless surface tensions α^* determined from Eq. (16) for ε/kT obtained from D_2 measurements – comparison with literature data.[25]

There are several potential explanations for this observation. First, heterogeneous nucleation may come into play, lowering the barrier to nucleation and thus reducing the effective surface tension. The most probable source of hetero-nuclei would arise from the initial precipitate. However, small angle X-ray scattering studies demonstrate that gelation is taking place from solutions where these precipitates have completely dissolved.[17,33]

A second reason the crystals may nucleate more rapidly stems from the quasi-one-dimensional nature of the nuclei. Consider the nucleus as a cylinder of length L and radius R; the free energy then becomes:

$$\Delta G = -\frac{\pi R^2 L}{4/3\pi a^3} kT \ln S + (2\pi R L \alpha_{side} + 2\pi R^2 \alpha_{end}) \qquad (18)$$

or in dimensionless form:

$$\Delta G^* = -\frac{3}{4} R^{*2} L^* \ln S + 2\pi R^* L^* \alpha^*_{side} + 2\pi R^{*2} \alpha^*_{end} \qquad (19)$$

where α^*_{side} and α^*_{end} are the surface tensions at the sides and ends of the cylinder, respectively. If R^* is independent of S, ΔG^* becomes either progressively more positive with increasing length (linear function in the second term) or progressively more negative with increasing length (linear function in the first term). At the supersaturation where ΔG^* drops below zero, this structural model of the nucleus predicts a critical nucleus that is the size of a monomer and no induction times will be observed.

This simplistic model demonstrates that changes of the critical nucleus structure can fundamentally change the barrier to nucleation. In a simulation study of growth of amyloid fibers, molecules were course grained as a rectangular cuboid with faces having three different interaction energies, and one face much more attractive than the other two. Fibers were nucleated but the nucleus appeared to require a three dimensional quality, suggesting the rectangular cylinder structural model may not reflect the structure of a critical nucleus.[47]

Allowing both the radius and the length to vary yields a nucleation barrier at a saddlepoint in the R^*-L^* plane (**Figure 11**) where $d(\Delta G^*)/dR^* = 0$ and $d(\Delta G^*)/dL^* = 0$, yielding:

$$R^*_c = \frac{8\pi}{3} \frac{\alpha^*_{side}}{\ln S} \qquad (20)$$

$$L^*_c = \frac{16\pi}{3} \frac{\alpha^*_{end}}{\ln S} \qquad (21)$$

This results in a nucleation barrier of $\Delta G^* \sim (\alpha^*_{side})^2 \alpha^*_{end}/(\ln S)^2$. The aspect ratio of the critical nucleus is then determined as $L_c^*/R_c^* = \alpha^*_{end}/\alpha^*_{side}$. We would expect the surface tension to be determined by the bond strength and the equilibrium fiber shape to be stabilized by low side surface tensions;[48] thus, we can assume $\alpha^*_{end}/\alpha^*_{side} = \varepsilon_{end}/\varepsilon_{side} = K$, where ε_{end} and ε_{side} are the bond energies gained when a molecule binds at the end or the side of a fiber. As D_2 measurements are made under dilute conditions, where the pair distribution function is dominated by the strongest strength of attraction, we assume $\varepsilon_{end}/kT \sim \varepsilon/kT$. With this assumption, the surface tension measured by induction times can be well approximated by $(1/K)^2(\varepsilon/kT)^3$. By relating the strength of attraction at the ends of the fiber to those obtained from D_2 measurements ($\varepsilon_{end} = \varepsilon$) and finding α^*_{end} from Eq. (17), the ratio K can be found from the slope of:

$$\ln t_{ind} = \frac{128\pi^3}{9}\frac{1}{K^2}\alpha_{end}^{*3}\frac{1}{(\ln S)^2} + \ln B \qquad (22)$$

For the measured water concentrations x_{H2O} = 0.25-0.40, the end/side ratio of the surface tensions takes values in the range K = 35-80, suggesting a decrease in the free energy barrier to nucleation of three orders of magnitude. As a consequence, the induction times observed at low to modest supersaturations for Fmoc-FF are substantially faster than those measured for crystallization of systems such as globular proteins.[25]

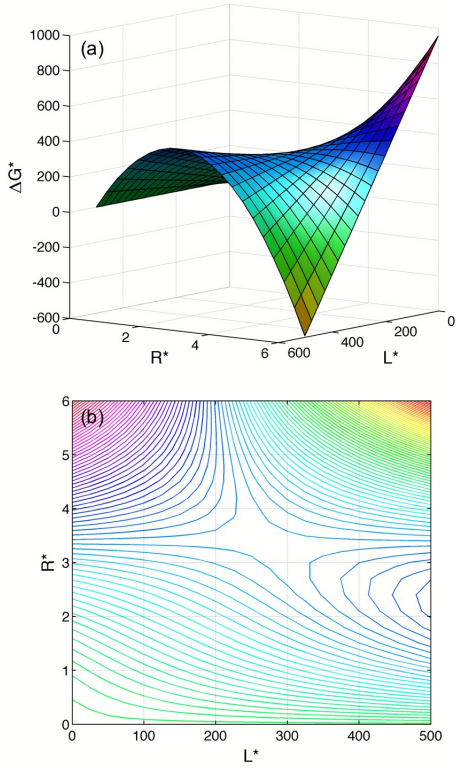

Figure 11. (a) The free energy barrier ΔG^* to the formation of a critical cylindrical nucleus in 3D space defined by a saddlepoint at critical size (R_c^*, L_c^*) at supersaturation S = 1.3, α_{end}^* = 4.23, K = 40; **(b)** Orthogonal projection onto the R^*-L^* plane.

Conclusions

Fmoc-FF molecules in mixtures of DMSO and water experience anisotropic interactions resulting in highly elongated crystals. The volume fraction dependence of the long-time self-diffusivity, characterizing molecular interactions, follows the phase behavior typical of crystallizing nanoparticles and molecules such as amino acids and globular proteins. Interpreting the experimentally determined diffusivity of Fmoc-FF using simple fluid theories allows for estimating the strength of attraction between the particles and relating it to water concentration. At the same average strength of attraction, broad classes of molecules display very similar solubilities. These results show that equilibrium behavior is dominated by the strongest attraction for particles that have a variety of attractive sites. On the other hand, we also show that at the same solubility (strength of attraction) and same supersaturation, the Fmoc-FF molecules nucleate crystals much faster than observed with less anisotropic molecules, indicating that nucleation is dominated by the weakest point of attraction. This allows us to conjecture that the greater the difference between the strengths of attraction of sites on a particle, the more anisotropic will the resulting crystalline phase be and the faster this phase will nucleate at the same average strength of attraction and supersaturation.

In understanding the full phase behavior of the Fmoc-FF/DMSO/H_2O system, we keep in mind that when initially mixed, precipitates are formed that are metastable to redissolution and the formation of a single stable phase, or are lost as fibers nucleate and grow.[17] We interpret this existence of a clearly metastable phase as arising from crossing the spinodal of a liquid-liquid phase boundary. Having large diffusivities, the Fmoc-FF molecules can rearrange quickly and attain a minimum free energy by crystallization. As a result, the metastable clusters are short-lived, and the location of the phase boundary cannot be captured quantitatively.

In light of the observations presented here, and taking into account the highly ordered molecular packing of Fmoc-FF molecules in the fibers, we conclude that the fibers can be treated as an equilibrium crystalline state arising from a first order phase transition of Fmoc-FF molecules upon the addition of water to the solution. The fibrillar nature of the crystals is attributed to the very different surface tensions on the faces of the resulting crystal, where we estimate that the ends of the fibers have surface tensions 30-80 times that of the fiber sides. The outcome of this imbalance is the formation of highly elongated crystals. Should solvent conditions be found where the interfacial tensions are closer in value we expect less elongated crystals and the loss of the ability of the Fmoc-FF to act as a gelator. This concept will be further explored in our following publications. When a fiber is broken by mechanical disruption, unfavorable surfaces are created, which initiates re-growth either by binding molecules that are free in solution or at the expense of a smaller fiber fragment by an Ostwald ripening-type process.

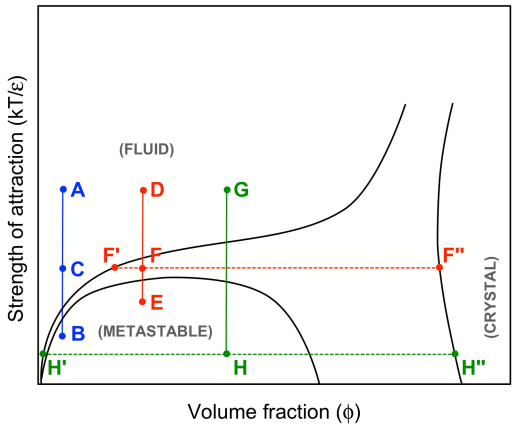

Figure 12. Proposed phase diagram for the Fmoc-FF/DMSO/H_2O system.

We propose that the Fmoc-FF/DMSO/H_2O system can be described by a phase diagram given in **Figure 12**. Below the supersaturation conditions ($S < 1$, point A in **Figure 12**), increasing attractions by adding a small amount of water will result in a quench into the spinodal (point B) due to high attractions in local regions. The amorphous clusters will redissolve as mixing effects take over and water is evenly distributed throughout the solution, and the system remains a colorless liquid solution (C).[32] At low to moderate water concentrations and supersaturations ($1 \le S < 10$, point D), increasing attractions will again result in an initial formation of an amorphous precipitate (E), followed by redissolution to point F in the crystal-liquid coexistence region, where nucleation occurs and a first order phase transition takes place (F', F"). Hence, the solution first turns opaque, then clear, and finally gels. At high supersaturations ($S > 10$) and water concentrations (G), a rapid quench to strong attractions places the system into the spinodal (H), and the fibers nucleate from the phase separated state (H', H"). This is observed as the solution turning opaque, gelling while still opaque, and then becoming translucent as the phase transition proceeds.[17]

In generalizing these results we suggest that molecular gelators can be considered as disks or short rods. The ability of these particles to form a fibrillar network will depend on the degree to which face-to-face interactions are preferred to side interactions. In the Fmoc-FF/DMSO/H_2O system, this imbalance of forces stems from the H_2O/DMSO ratio. Therefore, the anisotropic character of the formed structures will depend not only on the inherent nature of the gelling molecule, but also on how it interacts with the surrounding solvent.

Acknowledgements

This work was supported by the U.S. Department of Energy, Division of Materials Sciences, under Award no. DE-FG02-07ER46471 through the Frederick Seitz Materials Research Laboratory (FS-MRL) at the University of Illinois. The authors are grateful to Dr. Lingyang Zhu and Dr. Dean Olson for their valuable help with NMR experiments.

References

1 P. Terech and R. G. Weiss, *Chemical Reviews*, 1997, **97**, 3133-3160.
2 S. S. Babu, V. K. Praveen and A. Ajayaghosh, *Chem Rev*, 2014, **114**, 1973-2129.
3 R. V. Ulijn and A. M. Smith, *Chemical Society reviews*, 2008, **37**, 664-675.
4 V. Jayawarna, M. Ali, T. A. Jowitt, A. F. Miller, A. Saiani, J. E. Gough and R. V. Ulijn, *Advanced Materials*, 2006, **18**, 611-614.
5 A. M. Smith, R. J. Williams, C. Tang, P. Coppo, R. F. Collins, M. L. Turner, A. Saiani and R. V. Ulijn, *Advanced Materials*, 2008, **20**, 37-41.
6 C. Tang, A. M. Smith, R. F. Collins, R. V. Ulijn and A. Saiani, *Langmuir*, 2009, **25**, 9447-9453.
7 V. Jayawarna, S. M. Richardson, A. R. Hirst, N. W. Hodson, A. Saiani, J. E. Gough and R. V. Ulijn, *Acta biomaterialia*, 2009, **5**, 934-943.
8 A. Mahler, M. Reches, M. Rechter, S. Cohen and E. Gazit, *Advanced Materials*, 2006, **18**, 1365-1370.
9 R. Orbach, L. Adler-Abramovich, S. Zigerson, I. Mironi-Harpaz, D. Seliktar and E. Gazit, *Biomacromolecules*, 2009, **10**, 2646-2651.
10 R. Orbach, I. Mironi-Harpaz, L. Adler-Abramovich, E. Mossou, E. P. Mitchell, V. T. Forsyth, E. Gazit and D. Seliktar, *Langmuir*, 2012, **28**, 2015-2022.
11 J. Raeburn, G. Pont, L. Chen, Y. Cesbron, R. Lévy and D. J. Adams, *Soft Matter*, 2012, **8**, 1168.
12 J. Raeburn, C. Mendoza-Cuenca, B. N. Cattoz, M. A. Little, A. E. Terry, A. Z. Cardoso, P. C. Griffiths and D. J. Adams, *Soft Matter*, 2015, **11**, 927-935.
13 R. J. Mart, R. D. Osborne, M. M. Stevens and R. V. Ulijn, *Soft Matter*, 2006, **2**, 822.
14 S. Zhang, *Nature biotechnology*, 2003, **21**, 1171-1178.
15 S. Kim, J. H. Kim, J. S. Lee and C. B. Park, *Small*, 2015, **11**, 3623-3640.
16 L. Liu, K. Busuttil, S. Zhang, Y. Yang, C. Wang, F. Besenbacher and M. Dong, *Phys Chem Chem Phys*, 2011, **13**, 17435-17444.
17 N. A. Dudukovic and C. F. Zukoski, *Soft Matter*, 2014, **10**, 7849-7856.
18 H. Löwen, *Physics Reports*, 1994, **237**, 249-324.
19 S. Berghmans, J. Mewis, H. Berghmans and H. Meijer, *Polymer*, 1995, **36**, 3085-3091.
20 R. M. L. Evans, W. C. K. Poon and M. E. Cates, *Europhys Lett*, 1997, **38**, 595-600.
21 M. Muschol and F. Rosenberger, *The Journal of Chemical Physics*, 1995, **103**, 10424-10432.
22 B. Guo, S. Kao, H. McDonald, A. Asanov, L. L. Combs and W. William Wilson, *Journal of Crystal Growth*, 1999, **196**, 424-433.
23 B. L. Neal, D. Asthagiri and A. M. Lenhoff, *Biophysical Journal*, 1998, **75**, 2469-2477.
24 P. G. Vekilov, *Crystal Growth & Design*, 2004, **4**, 671-685.
25 A. M. Kulkarni and C. F. Zukoski, *Langmuir*, 2002, **18**, 3090-3099.
26 A. Y. Mirarefi and C. F. Zukoski, *Journal of Crystal Growth*, 2004, **265**, 274-283.
27 G. W. He, R. B. H. Tan, P. J. A. Kenis and C. F. Zukoski, *Journal of Physical Chemistry B*, 2007, **111**, 12494-12499.
28 D. F. Rosenbaum and C. F. Zukoski, *Journal of Crystal Growth*, 1996, **169**, 752-758.
29 D. Rosenbaum, P. C. Zamora and C. F. Zukoski, *Physical Review Letters*, 1996, **76**, 150-153.
30 S. Ramakrishnan and C. F. Zukoski, *The Journal of Chemical Physics*, 2000, **113**, 1237.
31 E. Zaccarelli, *Journal of Physics: Condensed Matter*, 2007, **19**, 323101.
32 N. A. Dudukovic and C. F. Zukoski, *Langmuir*, 2014, **30**, 4493-4500.
33 N. A. Dudukovic and C. F. Zukoski, *J Chem Phys*, 2014, **141**, 164905.
34 G. K. Batchelor and C. S. Wen, *J Fluid Mech*, 1982, **124**, 495-528.
35 D. J. Jeffrey and Y. Onishi, *J Fluid Mech*, 1984, **139**, 261-290.
36 B. Cichocki and B. U. Felderhof, *The Journal of Chemical Physics*, 1990, **93**, 4427.
37 P. Ertl, B. Rohde and P. Selzer, *J Med Chem*, 2000, **43**, 3714-3717.
38 W. S. Price, *Concept Magnetic Res*, 1997, **9**, 299-336.
39 Y. Cohen, L. Avram and L. Frish, *Angewandte Chemie*, 2005, **44**, 520-554.
40 T. M. Aminabhavi and B. Gopalakrishna, *J Chem Eng Data*, 1995, **40**, 856-861.

41 Y. Han, A. M. Alsayed, M. Nobili, J. Zhang, T. C. Lubensky and A. G. Yodh, *Science*, 2006, **314**, 626-630.
42 J. W. R. Morgan, D. Chakrabarti, N. Dorsaz and D. J. Wales, *Acs Nano*, 2013, **7**, 1246-1256.
43 S. Torquato and F. H. Stillinger, *Reviews of Modern Physics*, 2010, **82**, 2633-2672.
44 R. P. Sear, *The Journal of Chemical Physics*, 1999, **111**, 2001.
45 R. P. Sear, *Journal of Physics: Condensed Matter*, 2007, **19**, 033101.
46 J. J. De Yoreo and P. G. Vekilov, *Rev Mineral Geochem*, 2003, **54**, 57-93.
47 J. Zhang and M. Muthukumar, *J Chem Phys*, 2009, **130**, 035102.
48 T. P. Knowles, A. W. Fitzpatrick, S. Meehan, H. R. Mott, M. Vendruscolo, C. M. Dobson and M. E. Welland, *Science*, 2007, **318**, 1900-1903.

